Comparison of WRF Model-Simulated and MODIS-Derived Cloud Data

JASON A. OTKIN AND THOMAS J. GREENWALD

Cooperative Institute for Meteorological Satellite Studies, University of Wisconsin—Madison, Madison, Wisconsin

(Manuscript received 26 June 2007, in final form 19 September 2007)

ABSTRACT

In this study, the ability of different combinations of bulk cloud microphysics and planetary boundary layer (PBL) parameterization schemes implemented in the Weather Research and Forecasting Model to realistically simulate the wide variety of cloud types associated with an extratropical cyclone is examined. An ensemble of high-resolution model simulations was constructed for this case using four microphysics and two PBL schemes characterized by different levels of complexity. Simulated cloud properties, including cloud optical thickness, cloud water path, cloud-top pressure, and radiative cloud phase, were subsequently compared to cloud data from three Moderate Resolution Imaging Spectroradiometer (MODIS) overpasses across different portions of the domain. A detailed comparison of the simulated datasets revealed that the PBL and cloud microphysics schemes both exerted a strong influence on the spatial distribution and physical properties of the simulated cloud fields. In particular, the low-level cloud properties were found to be very sensitive to the PBL scheme while the upper-level clouds were sensitive to both the microphysics and PBL schemes. Overall, the simulated cloud properties were broadly similar to the MODIS observations, with the most realistic cloud fields produced by the more sophisticated parameterization schemes.

1. Introduction

Clouds are an important regulator of the earth's weather and climate system. For instance, radiative fluxes at the earth's surface are very sensitive to the cloud phase and to the vertical and horizontal distribution of cloud condensate. Surface precipitation and cloud-modified radiative fluxes affect the soil temperature and moisture content. Latent heat release associated with phase changes influences the large-scale circulation and can lead to explosive cyclogenesis. Cloud droplets and ice crystals also serve as effective locations for many atmospheric chemistry processes.

Because of the direct impact that clouds have on sensible weather conditions, it is critically important that numerical weather prediction (NWP) models realistically simulate their properties and structural evolution. Although substantial improvements have been made in recent years, cloud microphysical parameterization schemes remain one of the largest sources of uncertainty in NWP models. To realistically simulate cloud morphology, a microphysics scheme must be able to accurately represent numerous cloud processes and the complicated interactions that occur between different cloud species. Computational constraints, however, typically preclude the use of sophisticated bin microphysics schemes that are able to explicitly represent the evolution of the particle size distribution; therefore, it is necessary to utilize bulk schemes that are more efficient but also contain more approximations. Nonlinear interactions with the cumulus and planetary boundary layer (PBL) parameterization schemes, errors in the initial conditions, numerical diffusion, and the horizontal and vertical resolution also affect the simulated cloud structure, which complicates the diagnosis of biases in a microphysics scheme.

The scarcity of observations with fine temporal and spatial resolution renders it difficult to properly validate high-resolution model-simulated cloud data. Field studies provide a wealth of detailed information essential to understanding cloud processes but are generally limited to a specific time period and geographic location. Millimeter cloud radars also provide detailed cloud information, but again are limited to a specific location, typically over land. To validate regional or global model simulations, it is necessary to utilize cloud observations taken from geostationary or polar-orbiting satellite platforms. Satellite radiances and sat-

Corresponding author address: Jason A. Otkin, 1225 W. Dayton St., Madison, WI 53706.
E-mail: jason.otkin@ssec.wisc.edu

DOI: 10.1175/2007MWR2293.1

ellite-derived cloud products, such as cloud-top pressure (CTP), cloud optical thickness (COT), and cloud water path (CWP), are routinely available on a near-global basis from a variety of sensors. Although the accuracy of many satellite-derived datasets is generally too low to provide an absolute measure of the observed cloud properties (e.g., Zhang et al. 2005), such datasets are valuable for evaluating the realism of simulated cloud fields.

Prior studies have used satellite data to identify sensitivities in a model's microphysics scheme (Zhang et al. 2001; Chaboureau et al. 2002; Keil et al. 2003; Chaboureau and Pinty 2006), evaluate the accuracy of simulated cloud fields (Westphal et al. 1996; Yu et al. 1996; Garand and Nadon 1998; Klein and Jakob 1999; Mathieu et al. 1999; Chaboureau et al. 2000; Norris and Weaver 2001), conduct model intercomparison studies (Ryan et al. 2000; Webb et al. 2001), and validate operational forecast and climate models (Karlsson 1996; Rikus 1997; Tselioudis and Jakob 2002; Lopez et al. 2003; Sun and Rikus 2004). Overall, these studies have demonstrated the benefits of using satellite observations and a model-to-satellite approach to validate numerical model output. Many of these studies have also shown that the simulated cloud properties are highly sensitive to small changes in the microphysics scheme.

In this study, we will examine the ability of different combinations of cloud microphysics and PBL parameterization schemes implemented in the Weather Research and Forecasting (WRF) Model to realistically simulate the cloud properties associated with an extratropical cyclone that developed over the North Atlantic Ocean. Cloud data from an ensemble of high-resolution (4 km) model simulations will be compared to cloud products from three Moderate Resolution Imaging Spectroradiometer (MODIS) overpasses across different portions of the model domain. The paper is organized as follows. The algorithms used to generate the MODIS cloud products and WRF-simulated cloud data are discussed in section 2. This section also contains a detailed description of the microphysics and PBL schemes evaluated in this study. The model domain configuration and an overview of the observed cloud fields are presented in section 3. Results are shown in section 4, with conclusions presented in section 5.

2. Datasets and methodology

a. WRF model description

The WRF model is a sophisticated NWP model that solves the compressible nonhydrostatic Euler equations cast in flux form on a mass-based terrain-following vertical coordinate system. Prognostic variables include the horizontal and vertical wind components, various microphysical quantities, and the perturbation potential temperature, geopotential, and surface pressure of dry air. High-resolution global datasets are used to initialize the model topography and other static surface fields. A complete description of the WRF modeling system is contained in Skamarock et al. (2005).

Simulated cloud properties will be evaluated for four bulk microphysics schemes implemented in version 2.1.2 of the WRF model. The microphysics schemes vary in complexity from relatively simple single-moment schemes that explicitly predict the mixing ratio of each hydrometeor species to a more sophisticated double-moment scheme that predicts both the mixing ratio and number concentration. Each microphysics scheme contains prognostic equations describing the evolution of six hydrometeor species (water vapor, cloud water, rainwater, ice, snow, and graupel). The Purdue Lin (PLIN) and WRF single-moment 6-class (WSM6) schemes are single-moment schemes based on the work of Lin et al. (1983) and Rutledge and Hobbs (1984). Chen and Sun (2002) and Hong and Lim (2006) provide detailed descriptions of the PLIN and WSM6 schemes, respectively, which primarily differ in their treatment of ice microphysical processes. The Thompson (THOM) scheme is a hybrid single- and double-moment scheme that attempts to combine the computational efficiency of a single-moment scheme with the improved accuracy of a double-moment scheme (Thompson et al. 2006). Unlike the single-moment schemes, this scheme explicitly predicts both the mixing ratio and number concentration for cloud ice and uses a generalized gamma distribution to represent the particle size distribution for all species except snow. Following Field et al. (2005), the THOM scheme represents the snow particle size distribution as the sum of exponential and gamma distributions, and assumes a nonspherical snow particle shape with variable density. By allowing the user to specify a constant cloud-droplet number concentration, the THOM scheme also includes basic aerosol effects. The Seifert and Beheng (2005a,b) double-moment microphysics (SEIF) scheme includes prognostic equations for the mass and number densities of each hydrometeor species and is fundamentally different from the other microphysics schemes evaluated in this study. The SEIF scheme was specifically designed for use in high-resolution cloud-resolving model simulations and can discriminate between maritime and continental conditions. Although this scheme is computationally more demanding than the single-moment schemes, the inclusion of prognostic number concentrations should permit a more realistic simula-

tion of cloud microphysical processes. Warm-phase processes based on Seifert and Beheng (2001) account for turbulence effects, height-dependent fall speeds, and the collisional breakup of raindrops. Ice-phase processes are based on an improved Wisner et al. (1972) approximation for the collision integrals and include size-dependent mean collision efficiencies.

The structural evolution of the simulated cloud field is strongly coupled to the subgrid-scale temperature, moisture, and momentum fluxes generated by the PBL scheme. Modifications to the boundary layer thermodynamic and momentum profiles impact the growth and decay of low-level clouds and can also influence the vertical extent of deep convective clouds through changes in the vertical stability. To determine the influence that the PBL scheme exerts on the simulated cloud properties, model simulations were performed for each microphysics scheme using the Yonsei University (YSU; Hong et al. 2006) and Mellor–Yamada–Janjic (MYJ) PBL schemes. The YSU scheme includes an explicit treatment of entrainment processes at the top of the boundary layer, which is defined using a critical bulk Richardson number. Vertical fluxes are determined using a "nonlocal K" approach pioneered by Troen and Mahrt (1986). The MYJ PBL scheme is a nonsingular implementation of the Mellor and Yamada (1982) level 2.5 turbulence closure model. The scheme includes a prognostic turbulent kinetic energy (TKE) equation that accounts for TKE production and decay processes. Both PBL schemes are linked to a surface layer parameterization scheme based on Monin–Obukhov similarity theory (Monin and Obukhov 1954).

Simulated cloud properties, including COT, CWP, CTP, radiative cloud phase, and infrared brightness temperatures, were generated for each simulation. WRF model output, including the surface skin temperature, atmospheric temperature, water vapor mixing ratio, and the mixing ratio and effective particle diameters for each hydrometeor species, were ingested into the Successive-Order-of-Interaction forward radiative transfer model (Heidinger et al. 2006) in order to generate simulated top-of-atmosphere brightness temperatures. Gas optical depths were calculated for each MODIS infrared band using the Community Radiative Transfer Model. Ice cloud absorption and scattering properties were obtained from Baum et al. (2005), whereas the liquid cloud properties were based on Lorenz–Mie calculations. To closely mimic the MODIS CTP and cloud-phase products, the simulated brightness temperatures were passed through the operational MODIS algorithms (which will be described in section 2b). The simulated CWP was computed by vertically integrating the total microphysical mixing ratio (cloud water, rainwater, ice, snow, and graupel) within each grid column. Because of a strong sensitivity to the cloud phase, the COT was calculated separately for the liquid and frozen hydrometeor species, following the work of Han et al. (1995) and Heymsfield et al. (2003), respectively, and then combined into a single COT value.

b. MODIS cloud data

Flying onboard the Earth Observing System *Terra* and *Aqua* polar-orbiting satellite platforms, MODIS provides high-quality measurements in 36 spectral bands that were chosen to enable advanced studies of land, ocean, and atmospheric properties. The spatial resolution of each band varies from 250 to 1000 m at nadir, which is sufficient to characterize mesoscale cloud properties. Level 2 cloud data, with a spatial resolution of ~5 km, was used for this study. MODIS cloud products are part of an extensive processing framework that begins with the accurate calibration and geolocation of the broadband radiances. A probabilistic cloud mask is constructed for each MODIS granule using a series of multispectral tests (Ackerman et al. 1998). The CTP and effective cloud amount are subsequently inferred for each cloudy grid point using the CO_2-slicing algorithm, which is described in detail by Menzel et al. (2006). The thermodynamic phase near the cloud top is inferred using a bispectral infrared brightness temperature difference technique and the 11-μm brightness temperature (Ackerman et al. 1990; Strabala et al. 1994; Baum et al. 2000). This method is able to differentiate between ice, water, and mixed-phase clouds, as seen from a radiative transfer perspective. At this point in the processing framework, a series of tests are used to eliminate pixels that are not good candidates for optical property retrievals, such as pixels occurring along cloud edges or those characterized by partly cloudy conditions. The COT and effective particle radius are simultaneously retrieved for the remaining cloudy pixels using the observed reflectance at visible and near-infrared wavelengths and then comparing the results to theoretical calculations (e.g., Nakajima and King 1990). The retrieval method is especially accurate over dark ocean surfaces because the reflectance of the earth–atmosphere system arises primarily from light scattering by the cloud, with little influence from the underlying surface. Finally, the COT and effective radius calculations are used to infer the CWP.

3. Case study description

To avoid uncertainties associated with satellite-based cloud retrievals over land, an extratropical cyclone lo-

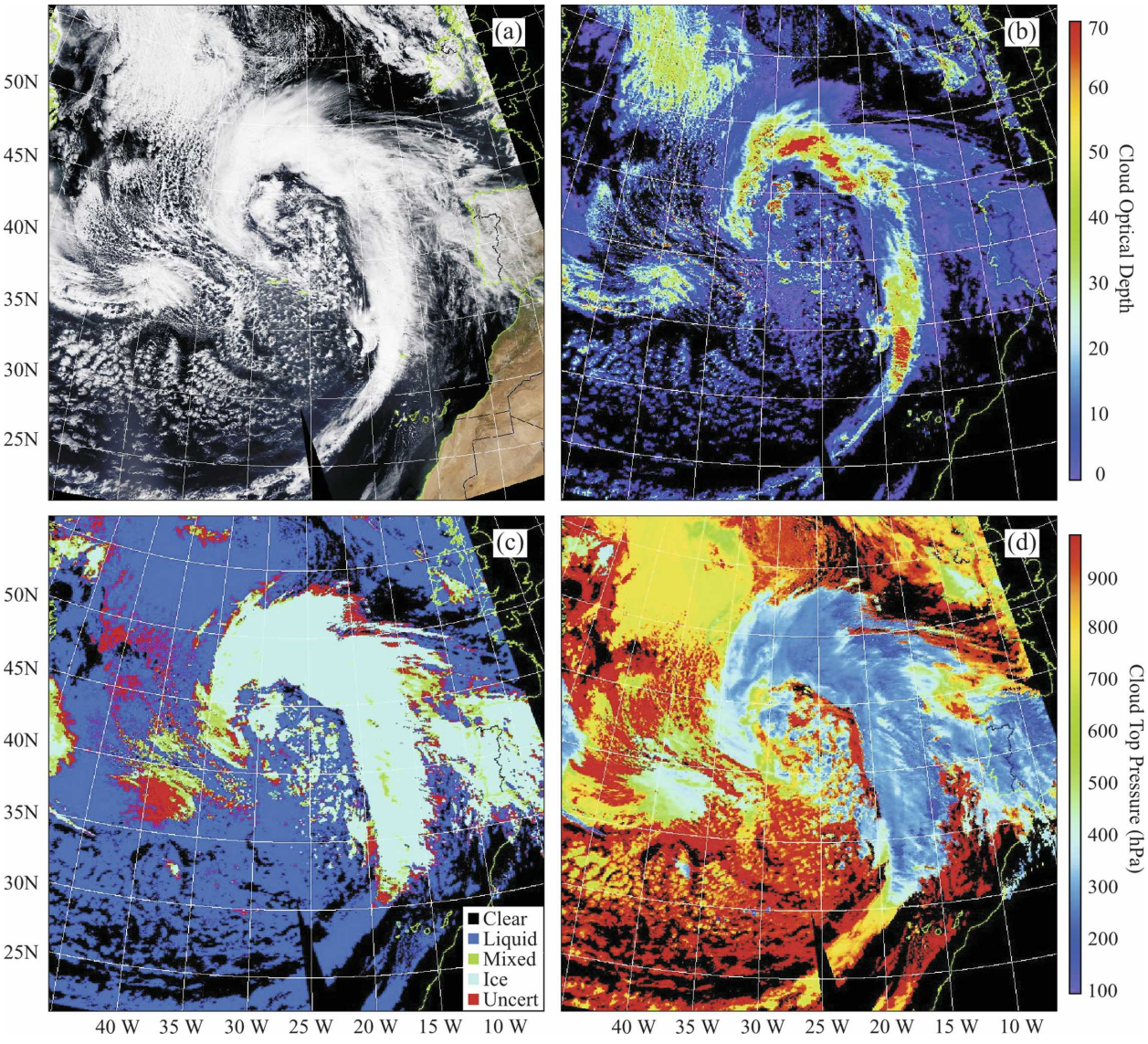

FIG. 1. Composite MODIS (a) visible imagery, (b) visible optical thickness, (c) cloud phase, and (d) cloud-top pressure (hPa) from the 1225–1235 and 1405–1415 UTC 24 Mar 2005 overpasses.

cated over the North Atlantic Ocean on 24 March 2005 was chosen for this study. Figure 1 shows the combined visible satellite imagery and derived cloud products for two successive MODIS overpasses over this region. The visible satellite imagery reveals a mature occluded cyclone characterized by a prominent comma-shaped cloud shield, with an extensive region of broken low-level cloud cover to the west and southwest. An arc of optically thick clouds extends around the northern periphery of the cyclone, with an additional band of deep convective clouds along the cold front. Optically thin cirrus clouds extend to the east of the cyclone with locally thicker clouds evident over the Iberian Peninsula. A thick stratocumulus cloud deck associated with an area of cold-air advection is also present to the northwest of the cyclone. The wide range of cloud types associated with this extratropical cyclone provides a valuable opportunity to evaluate the performance of the parameterization schemes for a complex real-world event.

A total of eight model simulations were performed for this case using the PBL and cloud microphysics schemes described in section 2a. Each simulation employed the Dudhia (1989) shortwave radiation and Rapid Radiative Transfer Model (RRTM) longwave radiation (Mlawer et al. 1997) schemes. Surface heat and moisture fluxes were calculated using the Noah land surface model. No cumulus parameterization

scheme was used; therefore, all clouds were explicitly predicted by the microphysics scheme. The simulations were initialized at 0000 UTC 24 March 2005 using 1° Global Data Assimilation System (GDAS) analyses and then run for 18 h on a single 1000 × 1000 gridpoint domain (Fig. 2), with 4-km horizontal grid spacing and 50 vertical levels. The vertical resolution decreased from less than 100 m in the lowest kilometer to ~700 m at the tropopause.

Three MODIS overpasses provided excellent coverage of the model domain (Fig. 2). The first overpass from 1225 to 1235 UTC passed directly over the deep convective clouds surrounding the cyclone. A second overpass from 1405 to 1415 UTC observed most of the cloud shield, including the thin cirrus clouds to the east of the cyclone. The final overpass from 1545 to 1550 UTC viewed the stratocumulus cloud deck and broken cloud cover in the western portion of the domain.

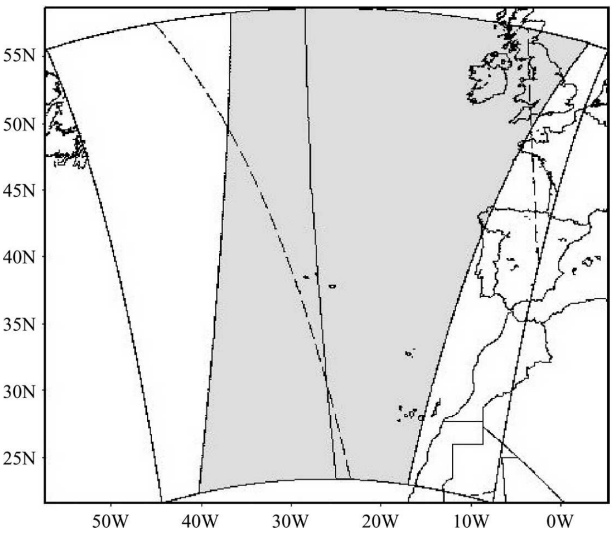

FIG. 2. Geographical coverage of each MODIS overpass is overlaid on the WRF model domain. The shaded area corresponds to the region observed by the 1225–1235 UTC MODIS overpass. The region observed by the 1405–1415 UTC MODIS overpass is located between the dashed lines. The region observed by the 1540–1550 UTC MODIS overpass is located between the western edge of the domain and the solid line running through the middle of the domain.

4. Results

Because cloud properties are strongly coupled to the large-scale circulation, we begin this section with a brief comparison of the observed and simulated synoptic conditions that occurred from 1200 until 1800 UTC 24 March 2005. For brevity, model results will only be shown for the SEIF–MYJ simulation. At 1200 UTC, the surface cyclone was embedded within a highly amplified baroclinic zone extending across the central Atlantic (Fig. 3a). Strong northwest winds combined with a sharp thermal gradient produced substantial cold-air advection within the southwestern quadrant of the cyclone. The surface cyclone was located beneath an upper-level shortwave trough that had rotated around the base of a zonally elongated large-scale trough over the central Atlantic (Fig. 3c). By 1800 UTC, the surface cyclone had deepened slightly as it slowly propagated to the northeast (Fig. 4a). Strong southerly winds ahead of the cyclone continued to amplify the downstream thermal ridge, which had become detached from the surface cyclone. The upper-level trough also deepened slightly, with strong winds persisting along its southern and eastern periphery (Fig. 4c). Inspection of the simulated data (Figs. 3, 4b,d) indicates that the location and magnitude of each of these features were realistically depicted during the model simulations.

As a first step in evaluating the realism of the model-simulated cloud fields, the observed and simulated 11-μm MODIS brightness temperatures are shown in Fig. 5. A detailed comparison of the datasets indicates that the PBL and cloud microphysics schemes both exert a strong influence on the spatial distribution of the simulated clouds. For instance, compared with the WSM6 and PLIN simulations, the upper-level cloud shield surrounding the extratropical cyclone covers a larger area when the SEIF and THOM microphysics schemes are used. Likewise, for a given microphysics scheme, slightly cooler brightness temperatures (indicative of higher cloud tops) occur within the cloud shield when the YSU PBL scheme is employed. The model simulations also exhibit substantial variability within the stratocumulus cloud region to the northwest of the cyclone. The MODIS brightness temperatures indicate that these clouds have a relatively uniform appearance over a large geographical region. The WSM6 and PLIN simulations, however, failed to reproduce these features, and are instead characterized by a heterogeneous cloud deck containing large, clear areas between the cumulus cells. By comparison, the THOM- and SEIF-simulated brightness temperatures have a more uniform appearance that better matches the observations. Simulations employing the YSU PBL scheme generally outperformed the MYJ scheme within this region, particularly for the SEIF and THOM simulations.

The finescale variability evident in Fig. 5 renders it difficult to apply a point-to-point comparison of the cloud datasets because small differences in location or timing can greatly impact standard statistical measures; therefore, probability distributions, which are less sensitive to phase errors, are employed for the remainder of the analysis. To limit the potentially adverse effects

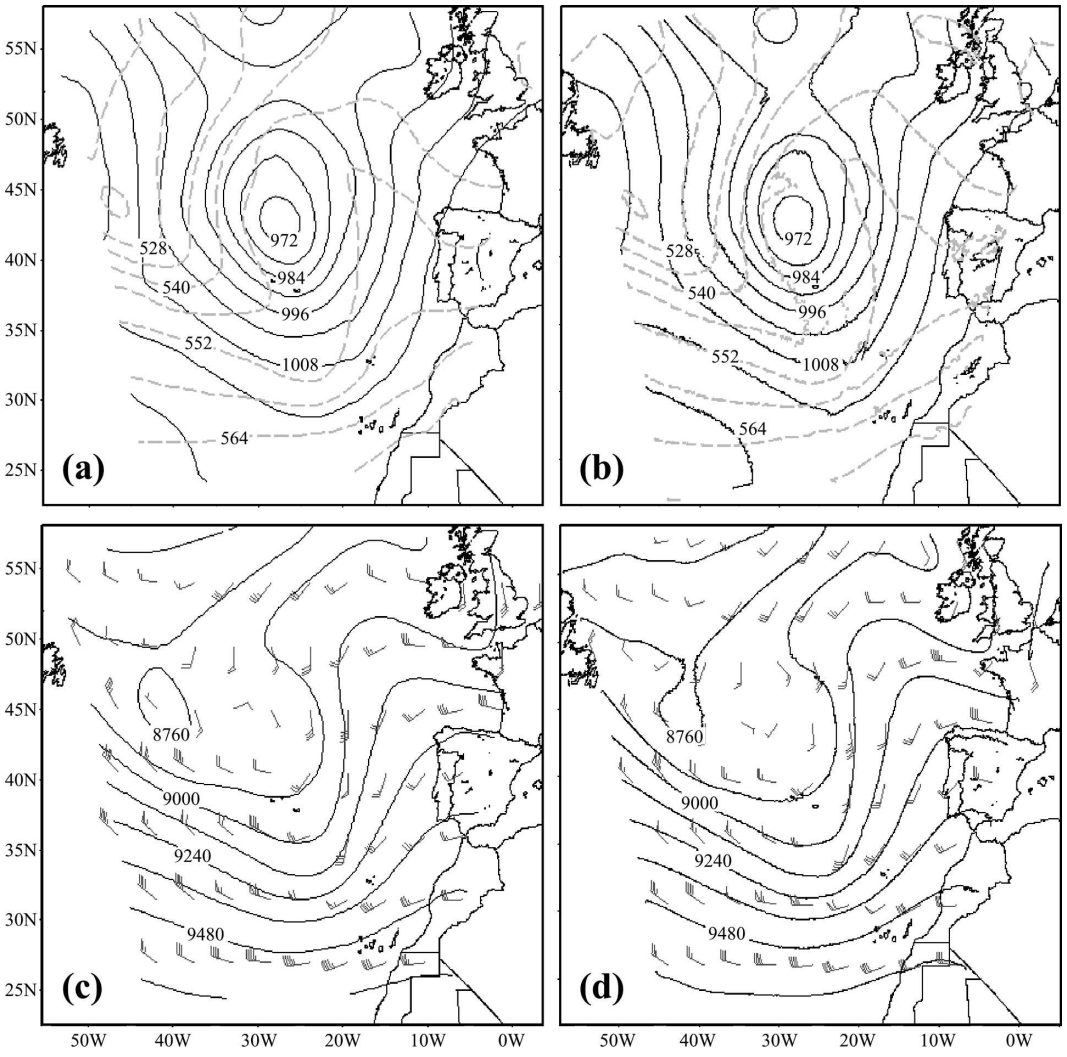

FIG. 3. (a) GDAS sea level pressure (hPa; solid line) and 1000–500-hPa thickness (m) analyses valid at 1200 UTC 24 Mar 2005. Sea level pressure is contoured every 6 hPa and labeled every 12 hPa. (b) As in (a), but for WRF-simulated data. (c) GDAS 300-hPa geopotential height (m; solid line) and wind (m s^{-1}) analyses valid at 1200 UTC 24 Mar 2005. Geopotential height is contoured every 120 m and labeled every 240 m. (d) As in (c), but for WRF-simulated data.

of the lateral boundary conditions on the simulated cloud properties, cloud data on the outermost 50 grid points around the edges of the model domain were excluded from the analysis. Model data located within each MODIS overpass swath at 1230, 1410, and 1550 UTC, respectively, along with the corresponding MODIS observations, were used for the subsequent analysis.

The simulated and observed COT–CTP probability distributions are shown in Fig. 6. As expected, the MODIS observations contain a wide range of cloud types, with three distinct maxima present in the distribution. The local maximum in the upper troposphere primarily corresponds to the deep convection and optically thin cirrus clouds surrounding the cyclone, the midlevel maximum corresponds to the stratocumulus cloud deck to the northwest of the cyclone, and the low-level maximum is primarily associated with the scattered cumulus clouds in the western and northeastern portions of the domain. All of the model simulations realistically capture the height of the upper-level clouds, though it is evident that the heights are too low for some of the optically thicker clouds (COT $>$ 30). The downward height bias is consistent with the slightly warmer brightness temperatures within the deep convection to the north and east of the cyclone center (see Fig. 5). Simulations employing the YSU PBL scheme generally contain more upper-level clouds than those

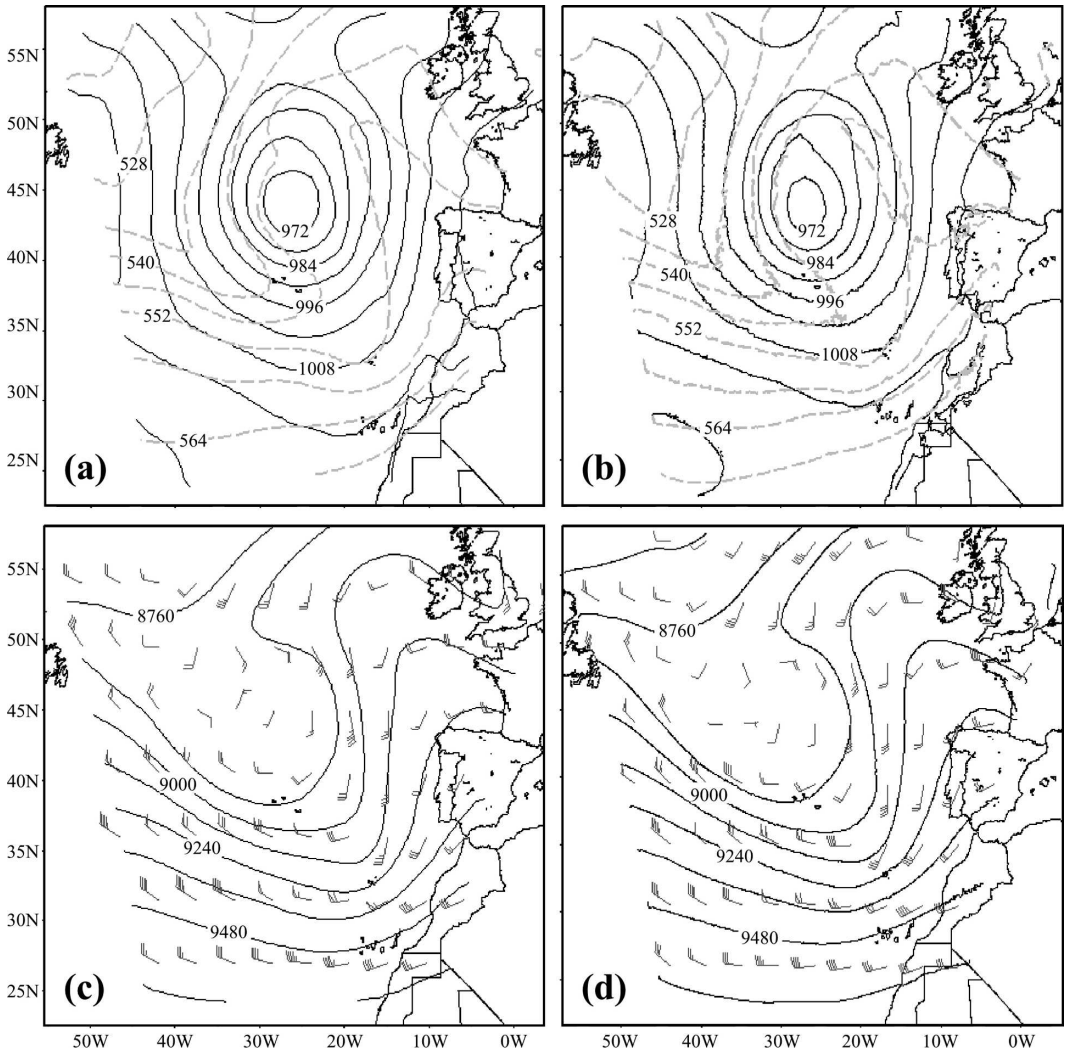

FIG. 4. As in Fig. 3, but valid at 1800 UTC 24 Mar 2005.

using the MYJ scheme, which indicates that the vertical fluxes generated by the PBL schemes affect all of the clouds in the column, not just those in the boundary layer. The midlevel maximum associated with the stratocumulus cloud deck is poorly predicted by all of the simulations except for the SEIF–YSU simulation. Inspection of the model data (not shown) reveals that the stratocumulus cloud deck is capped by a strong thermal inversion. Because satellite retrievals tend to overestimate the cloud-top height (underestimate the CTP) when an inversion is present, it is possible that part of the discrepancy is due to errors in the satellite CTP retrievals. However, because the CTP is retrieved with the same algorithm (although using brightness temperatures derived from very different sources), it is more likely that the discrepancy is due to inaccuracies in the PBL schemes. The warmer brightness temperatures to the northwest of the cyclone (see Fig. 5) indicate that the simulated cloud-top heights are too low relative to the observations. The lack of midlevel clouds suggests that the PBL schemes generate insufficient vertical mixing, which prevents the cloud-topped boundary layer from reaching its proper depth within this region. In the lower troposphere, the model simulations contain fewer (more) optically thin (thick) clouds than the MODIS dataset. Although simulations employing the MYJ PBL scheme tend to overestimate the optical thickness of the low-level clouds, it is clear that these simulations contain a more realistic depiction of the low-level clouds than those using the YSU PBL scheme. Given that neither PBL scheme is designed to explicitly represent shallow moist convection, the better performance of the MYJ scheme suggests that its treatment of dry turbulent mixing in the boundary layer, which in

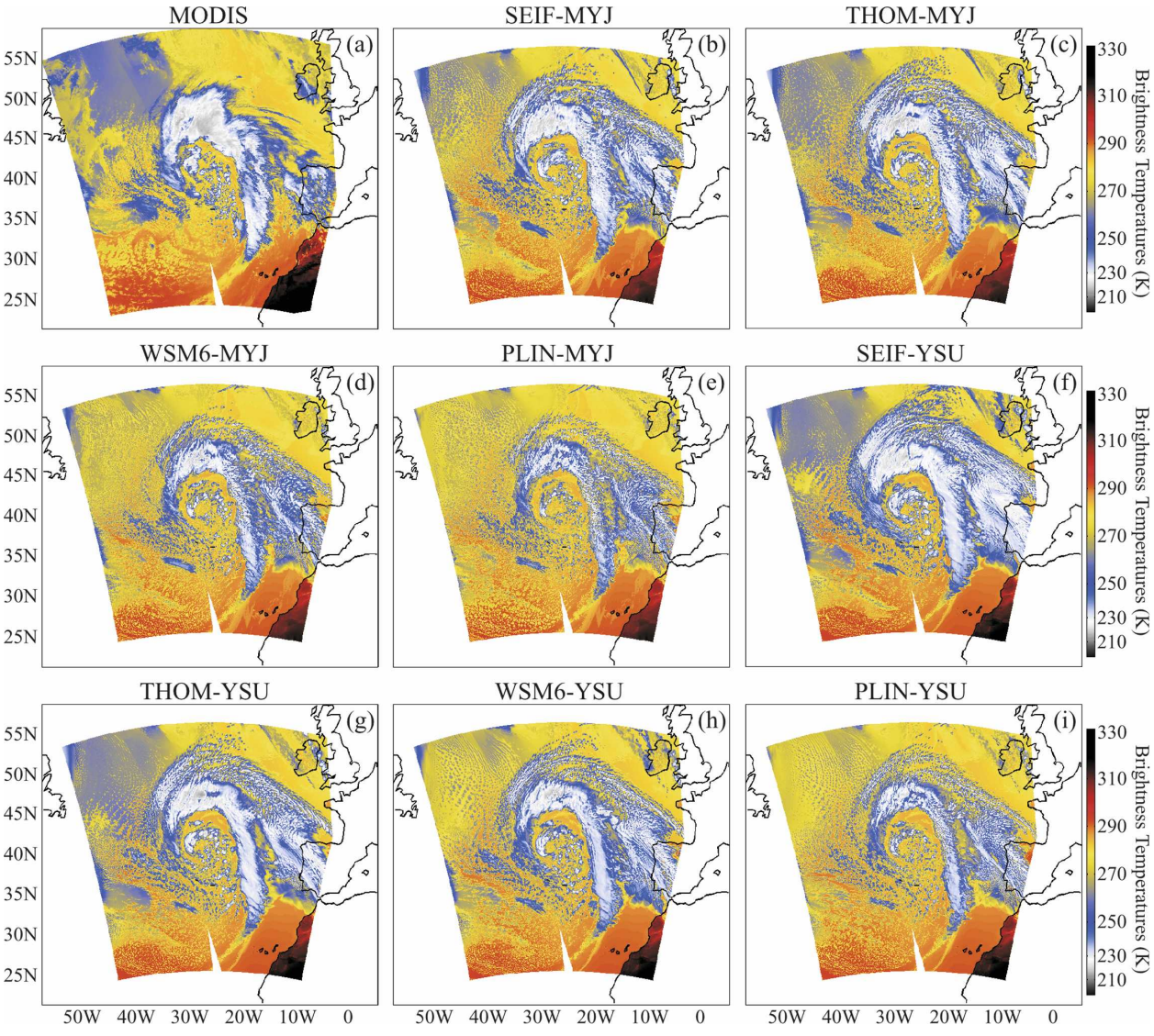

FIG. 5. (a) Composite MODIS 11-μm brightness temperatures (K) from the 1405–1415 and 1540–1550 UTC overpasses. Simulated MODIS 11-μm brightness temperatures (K) for the (b) SEIF–MYJ, (c) THOM–MYJ, (d) WSM6–MYJ, (e) PLIN–MYJ, (f) SEIF–YSU, (g) THOM–YSU, (h) WSM6–YSU, and (i) PLIN–YSU simulations.

turn influences the development of the low-level clouds, is better suited for high-resolution simulations.

The simulated and observed CWP–CTP probability distributions are shown in Fig. 7. Although the distributions are qualitatively similar to Fig. 6, the simulated CWP data more closely resemble the MODIS observations, particularly in the lower troposphere. A detailed inspection of the MODIS cloud data (not shown) revealed a tendency for relatively large effective radii to occur along the edges of optically thin cumulus clouds in the western portion of the domain. Because the CWP is proportional to both the COT and the effective radius, the improved agreement between the simulated and observed CWP datasets suggests that the MODIS COT retrievals are too small for some of the low-level cumulus clouds. Although this potential bias may account for some of the discrepancy between the simulated and observed COT distributions, the differences may also be due to biases in the simulated data. For instance, assuming that the microphysics scheme accurately predicts the CWP of the cumulus clouds, the simulated COT could still be too large if the corresponding effective radii are too small. This situation could occur either if the prescribed (or predicted) aerosol or cloud-droplet number concentrations are too high or if the assumed particle size distribution is inap-

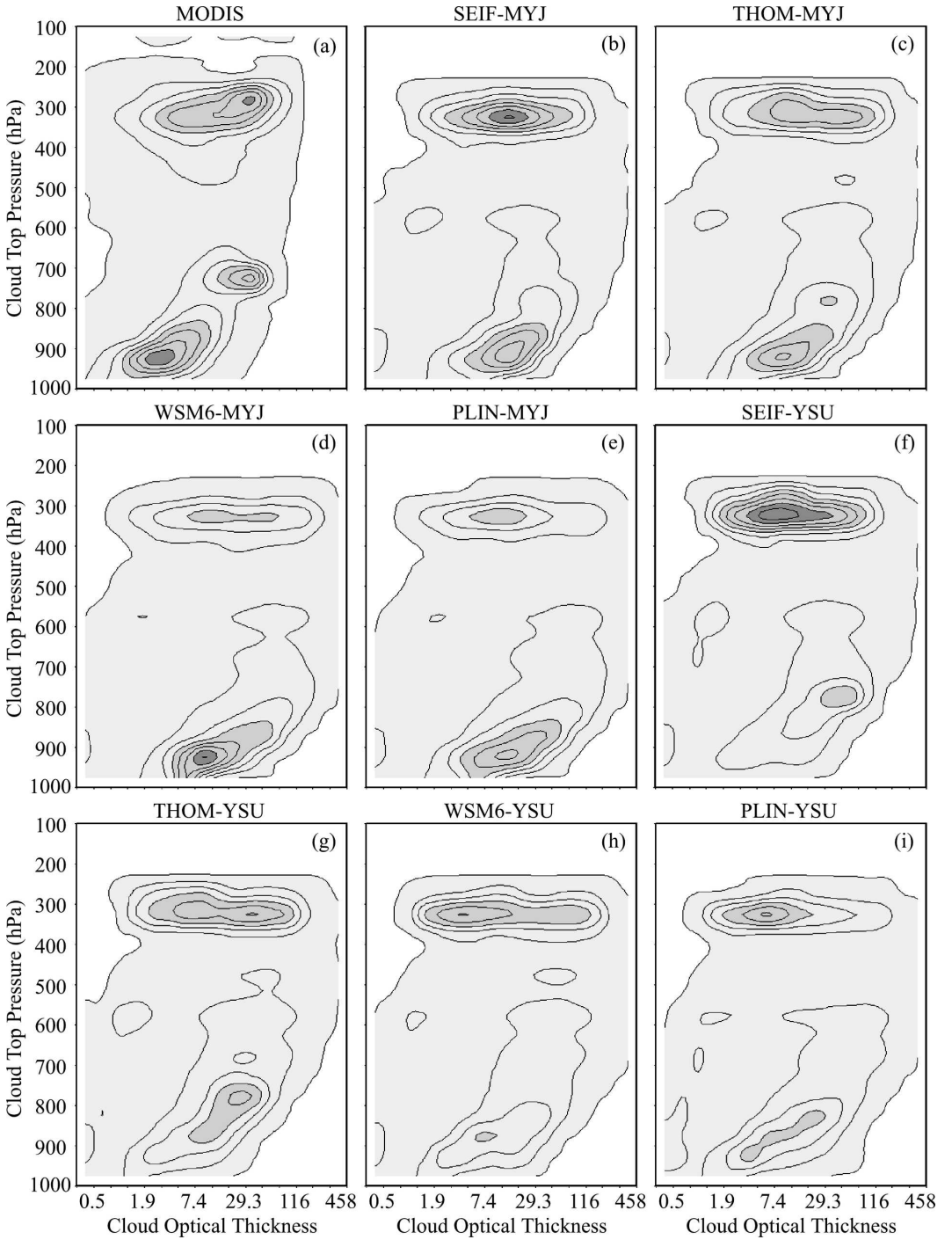

FIG. 6. Cloud optical thickness–cloud-top pressure (hPa) probability distributions contoured every 0.3% for the (a) MODIS observations and the (b) SEIF–MYJ, (c) THOM–MYJ, (d) WSM6–MYJ, (e) PLIN–MYJ, (f) SEIF–YSU, (g) THOM–YSU, (h) WSM6–YSU, and (i) PLIN–YSU simulations. Light, medium, and dark shading denote probabilities greater than 0%, 0.9%, and 1.8%, respectively.

propriate for cumulus clouds. Sensitivity tests using in situ cloud-droplet and aerosol measurements will be necessary to determine if this is the case. It should also be noted that the general tendency for the model simulations to generate low-level clouds characterized by excessive cloud condensate (both COT and CWP) relative to the MODIS observations suggests that the simulations may not be properly resolving the shallow cu-

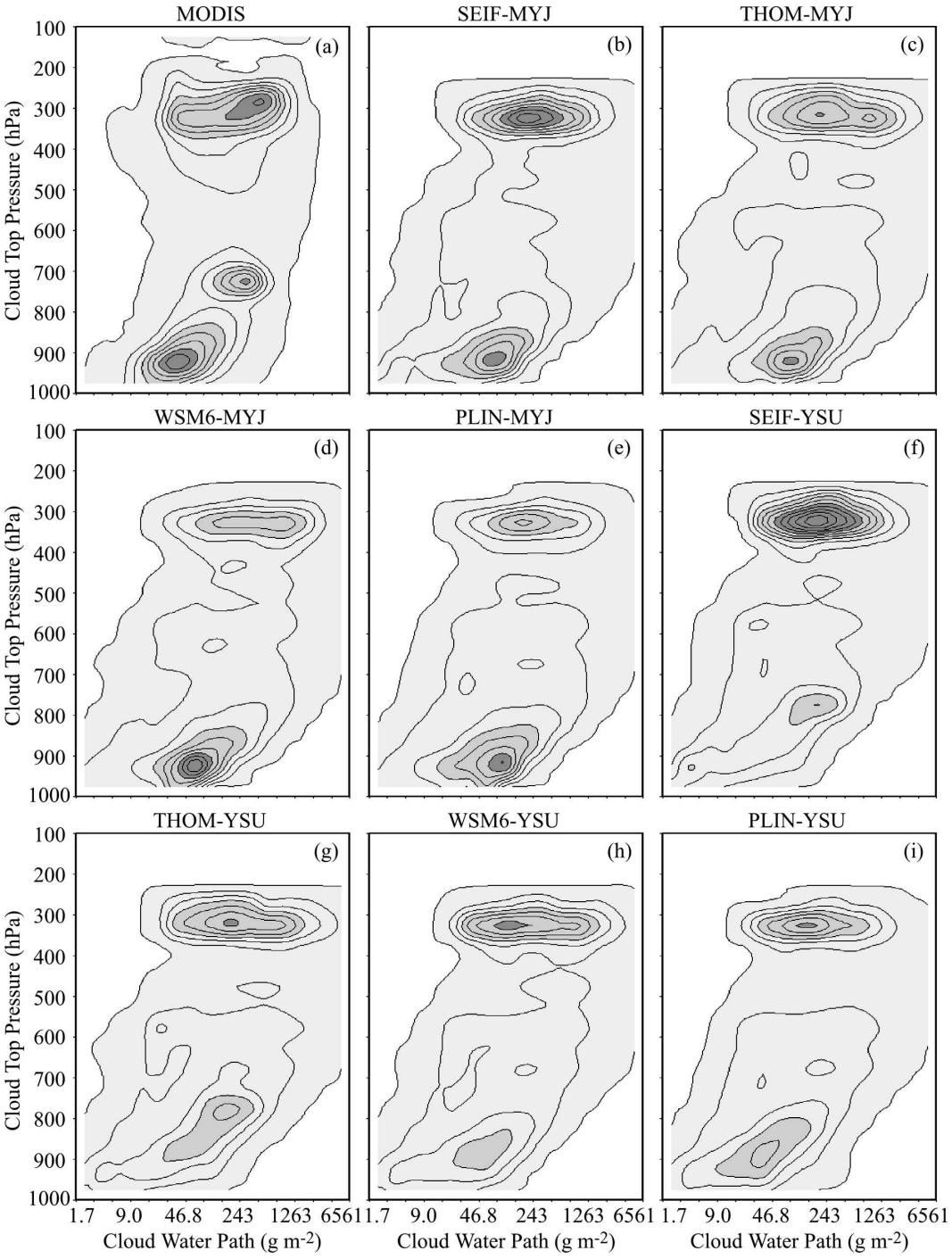

FIG. 7. Cloud water path (g m^{-2})–cloud-top pressure (hPa) probability distributions contoured every 0.3% for the (a) MODIS observations and the (b) SEIF–MYJ, (c) THOM–MYJ, (d) WSM6–MYJ, (e) PLIN–MYJ, (f) SEIF–YSU, (g) THOM–YSU, (h) WSM6–YSU, and (i) PLIN–YSU simulations. Light, medium, and dark shading denote probabilities greater than 0%, 0.9%, and 1.8%, respectively.

mulus clouds, which would not be unexpected given the small scale of the clouds relative to the model grid spacing.

Because differences in the simulated cloud-top pressure distributions complicate the evaluation of the simulated COT and CWP datasets, the total probability distributions for each variable are shown in Fig. 8. Overall, the model simulations generally contain fewer

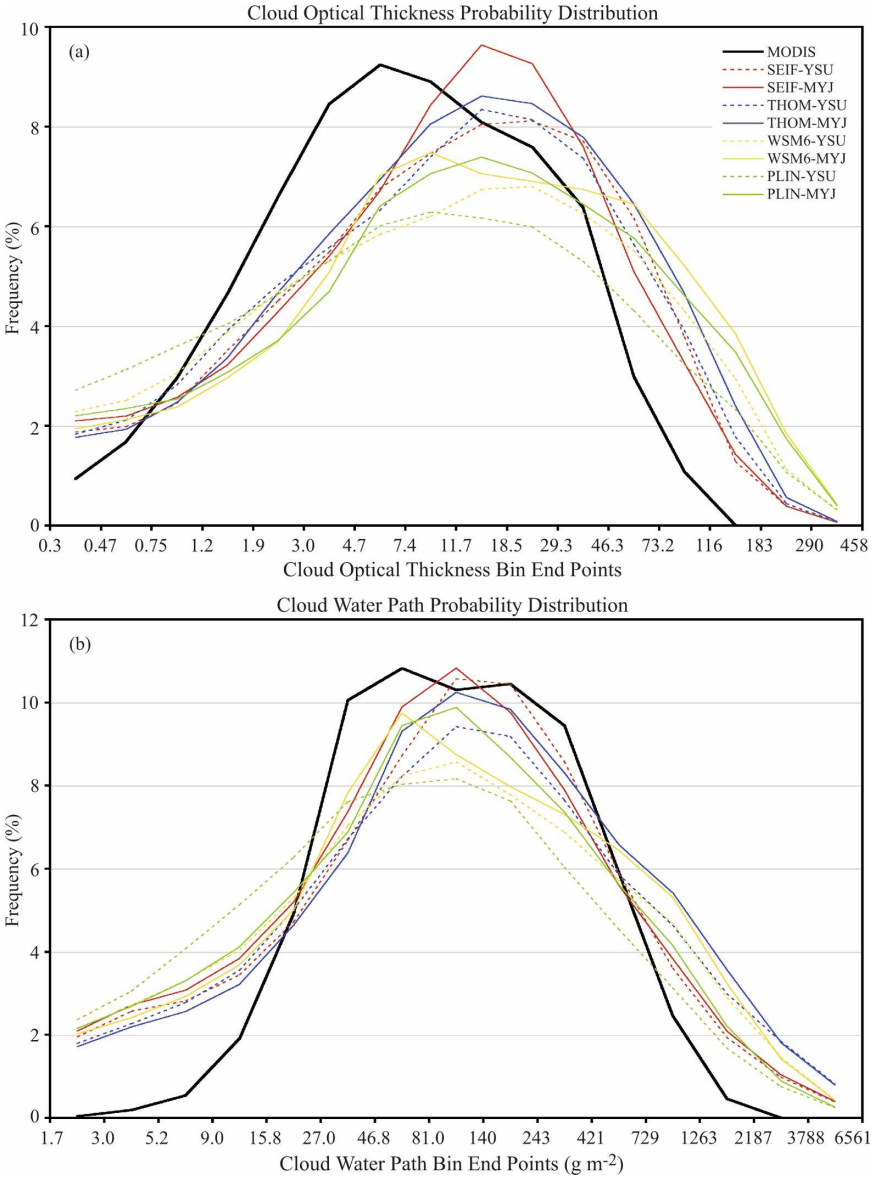

FIG. 8. Observed and simulated (a) cloud optical thickness probability distributions and (b) cloud water path probability distributions (g m^{-2}).

(more) optically thin (thick) clouds than the MODIS dataset. The tendency for the low-level clouds to be optically thinner in the MODIS dataset accounts for much of the discrepancy at the lower end of the distribution (COT $<$ 30). Although the microphysics schemes may overestimate the optical thickness of the simulated convective clouds (COT $>$ 40), it is more likely that the MODIS observations are too low because optical measurements saturate for thicker clouds. The simulated and observed CWP data (Fig. 8b) exhibit better agreement, although differences still exist across the entire distribution. For instance, the simulated datasets contain a higher frequency of clouds containing small quantities of cloud condensate (CWP $<$ 15), most of which occurred within the cumulus cloud region to the west of the cyclone. Without active in situ measurements, it is difficult to determine whether the relative abundance of these clouds either is due to a model bias, such as insufficient mixing in the boundary layer, excessive water vapor flux from the ocean surface, or the incomplete evaporation of small cloud droplets, or is simply due to the exclusion of partly cloudy and cloud edge pixels from the MODIS cloud property datasets. Overall, simulations employing the

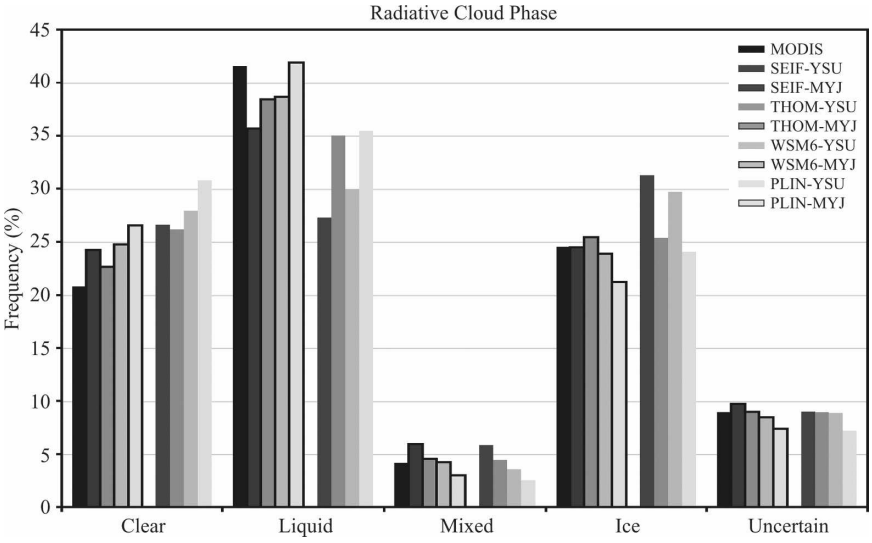

FIG. 9. Observed and simulated radiative cloud-phase probability distributions.

SEIF and THOM microphysics schemes or the MYJ PBL scheme were characterized by cloud properties that more closely matched the MODIS observations.

The simulated and observed radiative cloud-phase probability distributions are shown in Fig. 9. Comparison to the MODIS observations indicates that the simulated datasets generally contain fewer liquid clouds, a higher frequency of ice clouds and clear pixels, and a comparable number of mixed-phase and "uncertain" clouds. The inverse relationship between the simulated ice and liquid cloud frequencies partially arises from the varying size of the cloud shield surrounding the extratropical cyclone (see Fig. 5). Although the shielding effect of the upper-level cloud cover contributes to the lack of liquid clouds from the satellite perspective, the tendency for the model simulations to contain too many clear grid points accounts for the remainder of the discrepancy between the datasets. Simulations employing the YSU PBL scheme were characterized by the largest clear-sky and ice cloud biases, which resulted in a substantial underestimate of the liquid cloud occurrence. Inspection of the high-resolution (250 m) MODIS visible imagery revealed that the simulated datasets contain too many clear grid points between the larger cumulus cells in the western portion of the domain. Because the 5-km MODIS cloud-phase product utilizes radiance and reflectance data on a 1-km grid, the higher liquid cloud frequency indicates that the MODIS cloud product effectively captures the very small cumulus clouds within this region. The model simulations, however, are unable to accurately represent these clouds because the horizontal resolution is insufficient to explicitly resolve the processes that control their evolution. Although not examined in this study, the inclusion of a cumulus parameterization scheme may improve the model simulations through a better representation of the subgrid-scale cumulus clouds within these regions.

5. Conclusions

In this study, we examined the ability of different combinations of bulk cloud microphysics and PBL parameterization schemes implemented in version 2.1.2 of the WRF model to realistically simulate the wide variety of cloud types associated with an extratropical cyclone that developed over the North Atlantic Ocean. An ensemble of eight high-resolution (4 km) model simulations was constructed for this case using four microphysics and two PBL parameterization schemes characterized by different levels of complexity. Simulated cloud properties, including COT, CWP, CTP, radiative cloud phase, and infrared brightness temperatures, were subsequently compared to level 2 MODIS cloud data from three daytime overpasses across different portions of the domain. A detailed comparison of the simulated datasets demonstrated that both the PBL and cloud microphysics schemes exerted a strong influence on the simulated cloud properties. Overall, the model simulations realistically captured the height of the upper-level cloud shield surrounding the extratropical cyclone, though the cloud-top heights were too low for some of the optically thicker clouds. The areal extent of the cloud shield was largest for simulations employing either the YSU PBL scheme or the SEIF and THOM microphysics schemes. The shielding effect of

the upper-level cloud cover resulted in an inverse relationship between the relative occurrence of liquid and ice clouds for each simulation. The simulated cloud-phase probability distributions were strongly coupled to the PBL scheme, with the YSU simulations generally characterized by a higher frequency of ice clouds and clear-sky grid points, which resulted in a much lower frequency of liquid clouds relative to the MYJ simulations. The MODIS dataset contained fewer clear-sky pixels and more liquid clouds than the simulated datasets. Inspection of the high-resolution MODIS visible imagery revealed that the model simulations contained too many clear grid points within the cumulus cloud regions to the west of the cyclone, which indicates that the model was unable to accurately account for the small-scale cumulus clouds that occurred within these regions. The model simulations were also unable to properly simulate the cloud properties associated with a stratocumulus cloud deck to the northwest of the cyclone. The nearly complete lack of midlevel clouds in this region, especially for the MYJ simulations, suggests that the PBL schemes generated insufficient vertical mixing, which resulted in an unrealistically shallow cloud-topped boundary layer. Comparison of the total COT probability distributions revealed that the model simulations contained fewer (more) optically thin (thick) clouds than the MODIS dataset. The tendency for the low-level clouds to be optically thinner (thicker) in the MODIS (simulated) dataset accounts for much of the discrepancy at the lower end of the distribution (COT < 30). Although the microphysics schemes may have overestimated the optical thickness of the convective clouds (COT > 40), it is more likely that the MODIS retrievals underestimated their thickness because optical measurements saturate for thicker clouds. The total CWP probability distributions exhibited much better agreement with the MODIS observations, although the dynamic range was larger for the simulated datasets. Taken together, the results indicate that the most realistic cloud properties were obtained for simulations employing either the SEIF and THOM microphysics schemes or the MYJ PBL scheme. The strong sensitivity of the simulated cloud properties to the PBL scheme indicates that future microphysical parameterization studies need to pay special attention to the ability of the PBL scheme to realistically parameterize subgrid-scale vertical fluxes, and also illustrates the need for new PBL parameterization schemes that are appropriate for high-resolution model simulations.

Future work includes expanding this study to include different synoptic regimes and cloud types. We also plan to compare the simulated brightness temperature data to MODIS and Atmospheric Infrared Sounder (AIRS) observations in order to further evaluate the accuracy of the parameterized ice processes in the microphysics schemes. New PBL and microphysics schemes will also be evaluated as they become available in the WRF model.

Acknowledgments. Special thanks are given to Richard Frey for providing the MODIS cloud-top pressure retrieval algorithm and Mat Gunshor, Erik Olson, and Justin Seiglaff for generating the simulated MODIS brightness temperature datasets. Discussions with Axel Seifert and Greg Thompson were also appreciated. This work was funded under the National Oceanic and Atmospheric Administration Cooperative Agreement NA06NES4400002.

REFERENCES

Ackerman, S. A., W. L. Smith, J. D. Spinhirne, and H. E. Revercomb, 1990: The 27–28 October 1986 FIRE IFO Cirrus Case Study: Spectral properties of cirrus clouds in the 8–12 μm window. *Mon. Wea. Rev.,* **118,** 2377–2388.

——, K. I. Strabala, W. P. Menzel, R. A. Frey, C. C. Moeller, and L. E. Gumley, 1998: Discriminating clear sky from clouds with MODIS. *J. Geophys. Res.,* **103,** 32 141–32 157.

Baum, B. A., P. F. Soulen, K. I. Strabala, M. D. King, S. A. Ackerman, W. P. Menzel, and P. Yang, 2000: Remote sensing of cloud properties using MODIS Airborne Simulator imagery during SUCCESS. II. Cloud thermodynamic phase. *J. Geophys. Res.,* **105,** 11 781–11 792.

——, Y.-X. Hu, P. Yang, A. J. Heymsfield, S. Platnick, M. D. King, and S. T. Bedka, 2005: Bulk scattering properties for the remote sensing of ice clouds. Part II: Narrowband models. *J. Appl. Meteor.,* **44,** 1896–1911.

Chaboureau, J.-P., and J.-P. Pinty, 2006: Validation of a cirrus parameterization with Meteosat Second Generation observations. *Geophys. Res. Lett.,* **33,** L03815, doi:10.1029/2005GL024725.

——, J.-P. Cammas, P. Mascart, J.-P. Pinty, C. Claud, R. Roca, and J.-J. Morcrette, 2000: Evaluation of a cloud system life-cycle simulated by Meso-NH during FASTEX using METEOSAT radiances and TOVS-3I cloud retrievals. *Quart. J. Roy. Meteor. Soc.,* **126,** 1735–1750.

——, ——, ——, ——, and J.-P. Lafore, 2002: Mesoscale model cloud scheme assessment using satellite observations. *J. Geophys. Res.,* **107,** 4301, doi:10.1029/2001JD000714.

Chen, S.-H., and W.-Y. Sun, 2002: A one-dimensional time dependent cloud model. *J. Meteor. Soc. Japan,* **80,** 99–118.

Dudhia, J., 1989: Numerical study of convection observed during the winter monsoon experiment using a mesoscale two-dimensional model. *J. Atmos. Sci.,* **46,** 3077–3107.

Field, P. R., R. J. Hogan, P. R. A. Brown, A. J. Illingworth, T. W. Choularton, and R. J. Cotton, 2005: Parameterization of ice-particle size distributions for mid-latitude stratiform cloud. *Quart. J. Roy. Meteor. Soc.,* **131,** 1997–2017.

Garand, L., and S. Nadon, 1998: High-resolution satellite analysis and model evaluation of clouds and radiation over the Mackenzie Basin using AVHRR data. *J. Climate,* **11,** 1976–1996.

Han, Q., W. Rossow, R. Welch, A. White, and J. Chou, 1995: Validation of satellite retrievals of cloud microphysics and

liquid water path using observations from FIRE. *J. Atmos. Sci.,* **52,** 4183–4195.

Heidinger, A. K., C. O'Dell, R. Bennartz, and T. Greenwald, 2006: The succesive-order-of-interaction radiative transfer model. *J. Appl. Meteor. Climatol.,* **45,** 1388–1402.

Heymsfield, A. J., S. Matrosov, and B. Baum, 2003: Ice water path–optical depth relationships for cirrus and deep stratiform ice cloud layers. *J. Appl. Meteor.,* **42,** 1369–1390.

Hong, S.-Y., and J.-O. Lim, 2006: The WRF single-moment 6-class microphysics scheme (WSM6). *J. Korean Meteor. Soc.,* **42,** 129–151.

——, Y. Noh, and J. Dudhia, 2006: A new vertical diffusion package with an explicit treatment of entrainment processes. *Mon. Wea. Rev.,* **134,** 2318–2341.

Karlsson, K.-G., 1996: Validation of modeled cloudiness using satellite-estimated cloud climatologies. *Tellus,* **48A,** 767–785.

Keil, C., A. Tafferner, H. Mannstein, and U. Schattler, 2003: Evaluating high-resolution model forecasts of European winter storms by use of satellite and radar observations. *Wea. Forecasting,* **18,** 732–747.

Klein, S. A., and C. Jakob, 1999: Validation and sensitivities of frontal clouds simulated by the ECMWF model. *Mon. Wea. Rev.,* **127,** 2514–2531.

Lin, Y.-L., R. D. Farley, and H. D. Orville, 1983: Bulk parameterization of the snow field in a cloud model. *J. Climate Appl. Meteor.,* **22,** 1065–1092.

Lopez, P., K. Finkele, P. Clark, and P. Mascart, 2003: Validation and intercomparison of three FASTEX cloud systems: Comparison with coarse-resolution simulations. *Quart. J. Roy. Meteor. Soc.,* **129,** 1841–1871.

Mathieu, A., G. Seze, C. Guerin, H. Dupais, and A. Weill, 1999: Mesoscale boundary layer cloud structures as observed during the SEMAPHORE campaign. *Phys. Chem. Earth,* **8B,** 933–938.

Mellor, G. L., and T. Yamada, 1982: Development of a turbulence closure model for geophysical fluid problems. *Rev. Geophys. Space Phys.,* **20,** 851–875.

Menzel, W. P., R. A. Frey, B. A. Baum, and H. Zhang, 2006: Cloud top properties and cloud phase algorithm theoretical basis document. MODIS ATBD-MOD-04, 56 pp.

Mlawer, E. J., S. J. Taubman, P. D. Brown, and M. J. Iacono, 1997: Radiative transfer for inhomogeneous atmospheres: RRTM, a validated correlated-k model for the longwave. *J. Geophys. Res.,* **102,** 16 663–16 682.

Monin, A. S., and A. M. Obukhov, 1954: Basic laws of turbulent mixing in the surface layer of the atmosphere. *Contrib. Geophys. Inst. Acad. Sci., USSR,* **151,** 163–187.

Nakajima, T., and M. D. King, 1990: Determination of the optical thickness and effective particle radius of clouds from reflected solar radiation measurements. Part I: Theory. *J. Atmos. Sci.,* **47,** 1878–1893.

Norris, J. R., and C. P. Weaver, 2001: Improved techniques for evaluating GCM cloudiness applied to the NCAR CCM3. *J. Climate,* **14,** 2540–2550.

Rikus, L., 1997: Application of a scheme for validating clouds in an operational global NWP model. *Mon. Wea. Rev.,* **125,** 1615–1637.

Rutledge, S. A., and P. V. Hobbs, 1984: The mesoscale and microscale structure and organization of clouds and precipitation in midlatitude cyclones. Part XII: A diagnostic modeling study of precipitation development in narrow cold-frontal rainbands. *J. Atmos. Sci.,* **41,** 2949–2972.

Ryan, B. F., and Coauthors, 2000: Simulations of a cold front by cloud-resolving, limited-area, and large-scale models, and a model evaluation using in situ and satellite observations. *Mon. Wea. Rev.,* **128,** 3218–3235.

Seifert, A., and K. D. Beheng, 2001: A double-moment parameterization for simulating autoconversion, accretion, and self-collection. *Atmos. Res.,* **59–60,** 265–281.

——, and ——, 2005a: A two-moment cloud microphysics parameterization for mixed-phase clouds. Part 1: Model description. *Meteor. Atmos. Phys.,* **92,** 45–66.

——, and ——, 2005b: A two-moment cloud microphysics parameterization for mixed-phase clouds. Part II: Maritime vs continental deep convective storms. *Meteor. Atmos. Phys.,* **92,** 67–82.

Skamarock, W. C., J. B. Klemp, J. Dudhia, D. O. Gill, D. M. Barker, W. Wang, and J. G. Powers, 2005: A description of the Advanced Research WRF version 2. NCAR Tech. Note TN-468+STR, 88 pp.

Strabala, K. I., S. A. Ackerman, and W. P. Menzel, 1994: Cloud properties inferred from 8–12-μm data. *J. Appl. Meteor.,* **33,** 212–229.

Sun, Z., and L. Rikus, 2004: Validating model clouds and their optical properties using geostationary satellite imagery. *Mon. Wea. Rev.,* **132,** 2006–2020.

Thompson, G., P. R. Field, W. D. Hall, and R. M. Rasmussen, 2006: A new bulk microphysical parameterization for WRF & MM5. Preprints, *Seventh Weather Research and Forecasting User's Workshop,* Boulder, CO, NCAR, 5.3 [Available online at http://www.mmm.ucar.edu/wrf/users/workshops/WS2006/WorkshopPapers.htm.]

Troen, I., and L. Mahrt, 1986: A simple model of the atmospheric boundary layer sensitivity to surface evaporation. *Bound.-Layer Meteor.,* **37,** 129–148.

Tselioudis, G., and C. Jakob, 2002: Evaluation of midlatitude cloud properties in a weather and a climate model: Dependence on dynamic regime and spatial resolution. *J. Geophys. Res.,* **107,** 4781, doi:10.1029/2002JD002259.

Webb, M., C. Senior, S. Bony, and J.-J. Morcrette, 2001: Combining ERBE and ISCCP data to assess clouds in the Hadley Centre, ECMWF, and LMD atmospheric climate models. *Climate Dyn.,* **17,** 905–922.

Westphal, D. L., and Coauthors, 1996: Initialization and validation of a simulation of cirrus using FIRE-II data. *J. Atmos. Sci.,* **53,** 3397–3429.

Wisner, C., H. D. Orville, and C. Myers, 1972: A numerical model of a hail-bearing cloud. *J. Atmos. Sci.,* **29,** 1160–1181.

Yu, W., M. Doutriaux, G. Seze, H. Le Treut, and M. Desbois, 1996: A methodology study of the validation of clouds in GCMs using ISCCP satellite observations. *Climate Dyn.,* **12,** 389–401.

Zhang, M. H., and Coauthors, 2005: Comparing clouds and their seasonal variations in 10 atmospheric general circulation models with satellite observations. *J. Geophys. Res.,* **110,** D15S02, doi:10.1029/2004JD005021.

Zhang, Y., B. Rockel, R. Stuhlmann, R. Hollmann, and U. Karstens, 2001: REMO cloud modeling: Improvements and validation with ISCCP DX data. *J. Appl. Meteor.,* **40,** 389–408.